Nonlocal effects on the shock-augmented ignition scheme of laser inertial fusion

W. Q. Yuan,[1] Z. H. Zhao,[1] S. P. Zhu,[2] X. T. He,[2] and B. Qiao[1,3,*]

[1]*Center for Applied Physics and Technology, HEDPS, and SKLNPT, School of Physics, Peking University, Beijing 100871, China*

[2]*Institute of Applied Physics and Computational Mathematics, Beijing 100094, China*

[3]*Frontiers Science Center for Nano-optoelectronics, Peking University, Beijing 100094, China*

(Received 11 December 2023; accepted 5 March 2024; published 28 March 2024)

Shock-augmented ignition (SAI) has recently been proposed as a viable approach to optimize the shock ignition scheme of laser fusion, which may substantially reduce laser power and intensity requirements and, as a result, greatly inhibit the growth of laser-plasma instabilities. However, the nonlocal thermal transport effect, which is believed to play a significant role in shock ignition, has not been considered in evaluation of the SAI scheme yet. Here, by self-consistently including modeling of the space-time-dependent nonlocal thermal transport into the radiation hydrodynamic simulations, we revisit the whole implosion and ignition dynamics of SAI numerically and theoretically. We find that, due to the nonlocal effect, on the one hand, the time-delay window between the igniter spike and the compression pulse in the drive laser for achieving high-gain fusion is much broadened from about 0.45 to 0.7 ns, relaxing the difficulty of laser pulse shaping; on the other hand, both the coast time and the fusion burn duration are significantly reduced by, respectively, 0.22 ns and 47 ps, in favor of increasing the hot-spot pressure around the stagnation stage.

DOI: 10.1103/PhysRevResearch.6.013332

I. INTRODUCTION

Laser-driven inertial confinement fusion (ICF) is based on the spherical implosion of a small capsule driven by either thermal x-ray ablation (indirect-drive in a hohlraum) [1–6] or direct laser ablation (direct-drive) [7–10], where the spherical capsule is constructed with an outer layer of plastic (CH), a middle layer of deuterium-tritium (DT) ice fuel, and an inner region of DT gas. Due to the adiabatic spherical compression during implosion, combined with shock heating, the capsule finally evolves into a high-pressure hot spot at the center surrounded with a cold high-density fuel shell. Upon the stagnation stage, if both the compressed hot spot's temperature (T) and the fuel shell's areal density (ρR) are sufficient, the central hot spot ignites and efficiently burns the surrounding dense fuel shell, creating net energy release, which is so-called "ignition" [1,3]. A recent breakthrough at the National Ignition Facility (NIF) using an indirect-drive scheme, realizing both burning plasma and ignition with an energy gain of $G > 1$ [1,5], has excited the global fusion energy research community. However, in the indirect-drive scheme, laser energy must first be converted into thermal x rays in a gold hohlraum, leading to low-energy coupling efficiency and a limited energy gain of about $G < 15$ [11]. This makes the indirect-drive scheme less practical for future commercial fusion energy applications.

As the widely investigated scheme of direct-drive ICF, shock ignition (SI) [12–17] uses a sharp rise (spike) in laser power (intensity $I \sim 10^{16}$ W/cm^2) at the end of the drive laser pulse to launch a strong converging shock at the end of the compression phase. The converging shock is subsequently amplified in a collision with the rebound shock near the inner surface of the preassembled fuel shell, bringing further compression and heating of the hot spot and eventually resulting in "ignition." This additional shock compression and heating reduces the implosion velocity required for ignition and also reduces the susceptibility to Rayleigh-Taylor instability (RTI) as less acceleration is required. It has been shown theoretically [11,12] that SI has the potential for a low-ignition threshold and a high-energy gain combined with increased robustness to RTI. However, although the hydrodynamic advantages of SI are clear, it requires a high peak laser intensity of $I \sim 10^{16}$ W/cm^2, well above the thresholds of laser-plasma instabilities (LPIs), which means that SI faces great challenges in laser coupling efficiency reduction and fuel preheating by suprathermal electrons due to LPIs [17–19].

Most recently, shock-augmented ignition (SAI) [20,21] has been proposed as a viable approach to optimize SI, where a steep reduction in laser power is introduced preceding the sharp spike in power. The dip in the laser power preconditions the ablation plasma with both the electron temperature and the plasma pressure reduced, aiding shock formation driven by the following laser spike. Therefore, the required peak intensity of the drive laser (i.e., the maximum intensity of the spike) can be substantially reduced to 10^{15} W/cm^2, greatly inhibiting the growth of LPI. However, the nonlocal thermal transport effect arising from the existence of the steep-temperature-gradient region in laser-ablated plasmas [22–27], which is believed to play a significant role in the direct-drive scheme, particularly in SI [7,16,28,29], has not

*Corresponding author: bqiao@pku.edu.cn

yet been considered in Ref. [20] during evaluation of the key condition and performance of the SAI scheme.

In this paper, we revisit the whole implosion and ignition dynamics of SAI by self-consistently including modeling of the nonlocal thermal transport effect into the radiation hydrodynamic (rad-hydro) simulations. Since the electron thermal transport in laser-ablation dynamics is not only time-dependent but also space-varying, and strongly relevant to the *in situ* plasma conditions [30–32], we implement the space-time-dependent and multigroup Schurtz-Nicolaï-Busquet (SNB) nonlocal electron thermal transport model [26,27,33] into the rad-hydro code "FLASH" [34]. A series of simulation results shows that, due to the nonlocal preheating, the fuel shell becomes no longer near-isentropic during implosion, whose adiabat is increased by about 50%. Moreover, the compression shock velocity also increases and the shock rebounds earlier, which induces the collision between the rebounding shock and the igniter shock occurring at a place farther away from the inner surface of the fuel shell. These modifications of the implosion dynamics eventually result in two key different evaluations of SAI. On the one hand, the time-delay window between the igniter spike and the compression pulse in the drive laser for achieving high-gain fusion is much broadened from about 0.45 to 0.7 ns, relaxing the difficulty of laser pulse shaping in SAI. On the other hand, both the coast time and the fusion burn duration are significantly reduced by, respectively, from 1.72 ns down to 1.5 ns for the former and from 90 to 43 ps for the latter, in favor of increasing the hot-spot pressure around the stagnation stage against radiation cooling and plasma expansion.

II. SIMULATION SETUP

The rad-hydro simulations are performed in the one-dimensional spherical geometry for SAI. Figure 1(a) shows schematically the implosion capsule design, which consists of a 51-μm wall CH ablator, a 165-μm-thick DT-ice layer, and a 1535-μm-radius DT gas with a mass density of 6.2×10^{-4} g/cm^3. Meanwhile, the SAI pulse shape (the red line) with an energy of 2.0 MJ and a wavelength of 0.351 μm is presented in detail, which has a 3.6-TW foot and rises to a peak compression power of 365 TW, followed by a 0.7-ns dip at a power of 130 TW and a 0.9-ns igniter spike at a power of 510 TW. The corresponding peak intensities of the compression pulse and the igniter spike are respectively 0.93×10^{15} and 1.3×10^{15} W/cm^2. The size of the simulation box is 3000 μm, divided into 7200 cells and the time step is small enough (typically $\sim 10^{-14}$ s) to meet the Courant-Friedrichs-Lewy stable condition and even resolve the electron-ion collision time. It should be pointed out that the SNB model has included the improvements in Refs. [27,33], such as modifying the Krook collision operator and properly considering the electric field correction to the mean-free-path, which basically eliminate the overestimation of preheating in the original SNB model [26]. For simulations with the improved multigroup SNB model, 20 energy groups equal-spaced in logarithms are selected, and more energy groups give identical results. Furthermore, the simulation results are compared with those by the same flux-limited Spitzer-Härm (SH) model as Ref. [20] with the constant flux limiter $f = 0.06$, where the simulating thermal flux is chosen as $Q = \min(Q_{\rm SH}, fQ_{\rm fs})$ and $Q_{\rm fs}$ is the free-stream thermal flux [35,36].

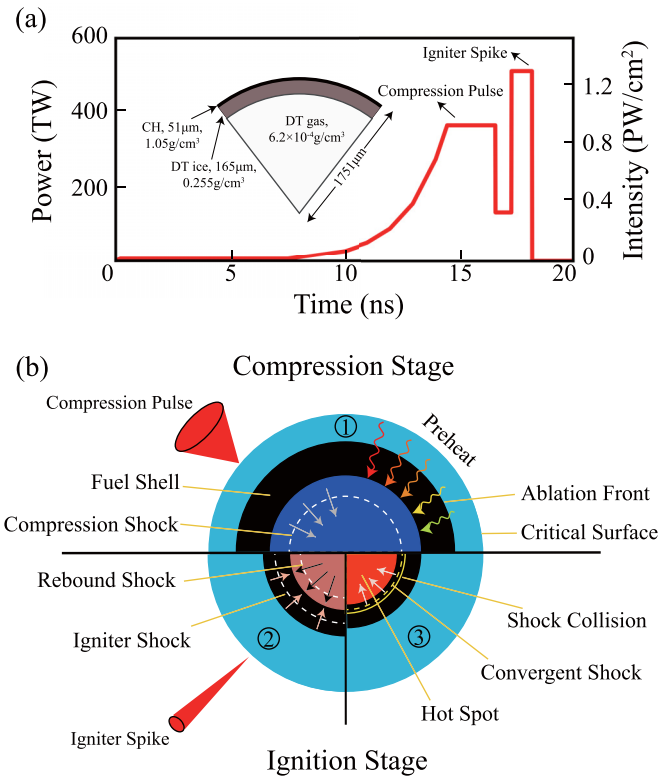

FIG. 1. Schematics of the shock-augmented ignition (SAI) and the nonlocal effects during the whole SAI dynamics. (a) The SAI laser pulse shape with an energy of 2.0 MJ (red line), which has a 3.6-TW foot and rise to a peak compression power of 365 TW, followed with a 0.7-ns dip at a power of 130 TW and a 0.9-ns igniter spike at a power of 510 TW. Inset: Implosion capsule with the plastic (CH) ablator, which has a 1751-μm outer radius and a 1.39-mg total DT fuel mass. (b) The separated compression (upper half, label 1) and ignition (lower half, labels 2 and 3) stages for SAI (labels 1, 2, and 3 represent the order of the stages): in the compression stage, the DT fuel shell is compressed and accelerated by the compression pulse, with the fluctuating arrows (right) representing that the nonlocal thermal flux preheats the fuel shell; in the ignition stage, the igniter shock (pink arrows) collides with the rebound shock (black arrows), which generates a convergent shock (white arrows) to further compress and heat the hot spot, with the nonlocal thermal transport effect influencing the shock velocities and the position of the shock collision.

III. THE COMPRESSION DYNAMICS

Figure 2 shows simulation results of the SAI compression dynamics after taking the nonlocal thermal transport effect into account. Figure 2(a) presents $\nabla \ln P$ in the time-radius plane during implosion, where we can see that the compression shock breaks out from the inner surface of the DT ice shell at ~10 ns and the compression stage lasts from 10 ns to about 18 ns. The thermal flux and the mass density around the fuel shell at 16 ns are exhibited in Fig. 2(b). We see clearly that the fuel shell is significantly preheated after considering the nonlocal effect, with the thermal flux approximately 5

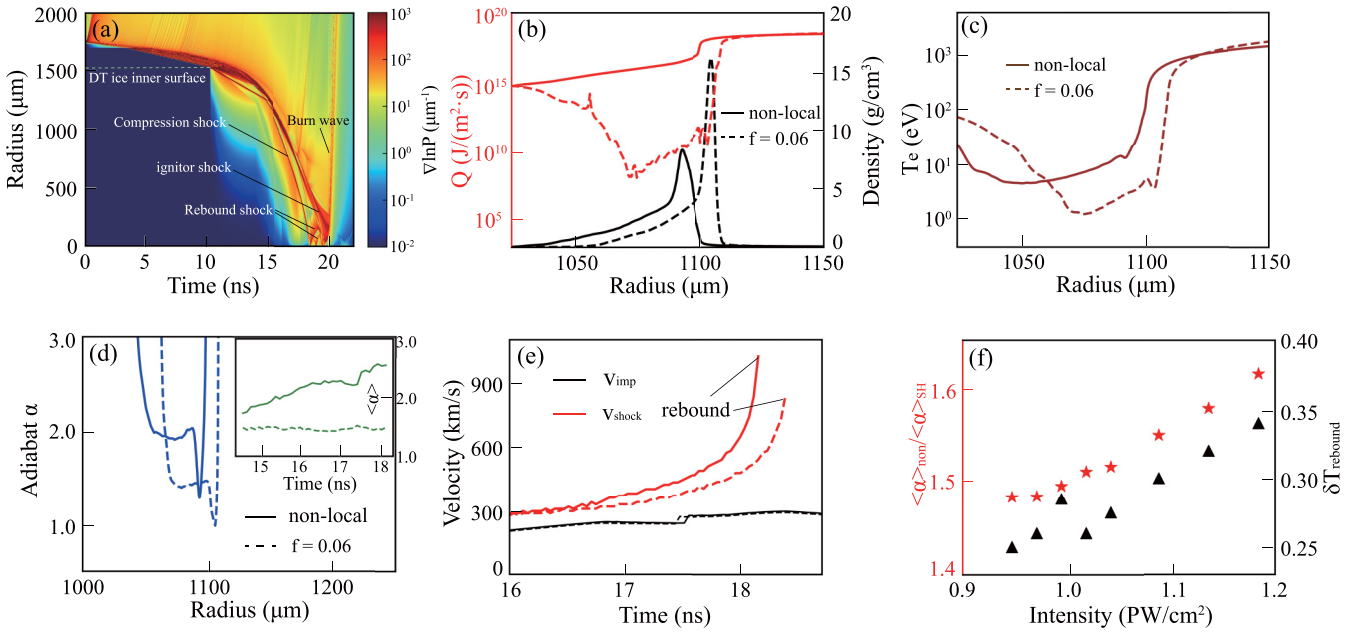

FIG. 2. The simulation results of the compression dynamics for SAI after taking the nonlocal thermal transport effect into account. (a) The reciprocal of the pressure gradient scale length ($\nabla \ln P$) during the implosion in the time-radius plane, where we can see that the compression shock breaks out from the inner surface of the DT ice shell at ∼10 ns, with the compression stage from 10 ns to about 18 ns. (b) Distribution of the thermal flux (red lines) and the mass density (black lines) at 16 ns for simulations considering the nonlocal effects (solid lines) compared with that by flux limited SH model with $f = 0.06$ (dashed lines), where the preheating in the fuel shell and subsequent density reduction are shown clearly. The positions of the density peaks represent the center of the fuel shell. (c) Distribution of the electron temperature around the fuel shell at 16 ns, with the temperature of the fuel shell by nonlocal model (solid line) approximately twice of that by the flux-limited SH model (dashed line). (d) Distribution of the adiabat α (blue lines) around the fuel shell at 16 ns, with the inset displaying the evolution of the spatial-average adiabats $\langle\alpha\rangle$ (green lines) from 14.6 to 18 ns. (e) Evolution of the implosion velocity of the fuel shell (black lines) and compression shock velocity (red lines) before rebound by the nonlocal model (solid lines) and flux-limited SH model (dashed lines). (f) The ratio $\langle\alpha\rangle_{\rm non}/\langle\alpha\rangle_{\rm SH}$ (red stars) between the spatial-average adiabats by the nonlocal model and the flux-limited SH model at the end of the compression stage of 18 ns and the time interval $\delta T_{\rm rebound}$ (black triangles) between the rebounding time of compression shocks by the two models vary with the laser intensity from 0.93×10^{15} to 1.16×10^{15} W/cm^2.

orders of magnitude higher than that in the case by using the flux-limited SH model. Correspondingly, the compression of the fuel shell is reduced and the peak density is almost halved from 17 to 9 g/cm^3. Meanwhile, due to the preheating, the electron temperature of the fuel shell is nearly doubled, as shown in Fig. 2(c), which further increases the entropy and breaking the near-isentropic condition. As shown in Fig. 2(d), the adiabat of the entire shell is increased by about 30%. And the spatially averaged adiabat $\langle\alpha\rangle$ is increased gradually with time from 1.6 to 2.5 during the compression stage, unlike the constant low-adiabat of ∼1.45 in the flux-limited SH model ($f = 0.06$). In short, the near-isentropic condition for SAI during the compression stage [20] is broken by preheating due to the nonlocal thermal transport, which further leads to the reduction of fuel shell compressibility.

Figure 2(e) shows the time evolution of the implosion velocity of the fuel shell and the compression shock velocity before rebound. We see that, comparing with those using the flux-limited SH model, the implosion velocity (black lines) is basically unaffected after taking into account the nonlocal effect, but the compression shock velocity (red lines) is observably increased. Moreover, the closer to the capsule center the place is, the more the increase of the shock velocity is. This results in an earlier rebound of the compression shock by about $\delta T_{\rm rebound} \sim 0.25$ ns, whose value is even comparable to the high-gain time window of ∼0.5 ns of SAI in Ref. [20]. Figure 2(f) shows the implosion dynamics for different compression pulse intensities. We see that, on the one hand, the spatially averaged adiabat at the end of the compression stage (18 ns) is increased by more than 50% after considering the nonlocal effect and this increase becomes more pronounced when the compression pulse intensity increases. On the other hand, the rebound time of the compression shock also becomes earlier when the compression pulse intensity increases.

IV. THE IGNITION DYNAMICS

These modifications of the compression dynamics subsequently affect the ignition dynamics. Figure 3(a) presents the mass density profiles (red lines) of the fuel shell by the nonlocal model at 19.0 ns (solid) and the flux-limited SH model at 19.3 ns (dashed) before the collision between the igniter shock and the rebound shock. We see that, in comparison with that using the flux-limited SH model, the rebound shock collides with the igniter shock at a place farther away from the inner surface due to its earlier rebound because of the nonlocal effect. Thus, more fuel can be swept by the convergent shock after the shock collision and further be compressed and heated, which is beneficial for achieving the ignition conditions. Meanwhile, the inset of Fig. 3(a) demonstrates that the

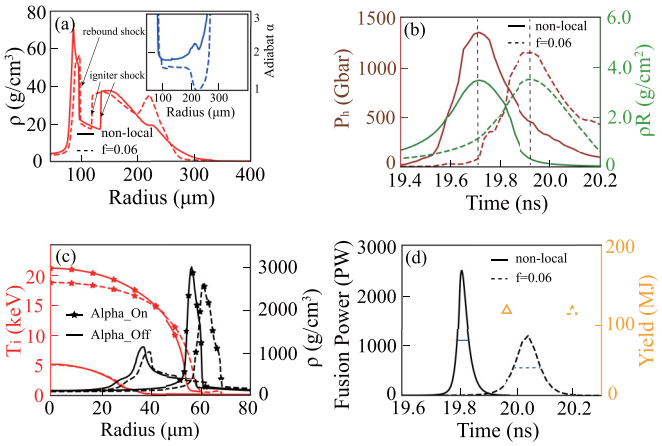

FIG. 3. The simulation results of the ignition dynamics for SAI after considering the nonlocal thermal transport effect. (a) Density profiles (red lines) of the fuel shell before the occurrence of shock collision by the nonlocal model at 19.0 ns (solid line) and the flux-limited SH model at 19.3 ns (dashed line), with the corresponding adiabats (blue lines) shown in the inset. (b) Evolution of the hot-spot pressure (P_h, brown lines) and shell area density (ρR, green lines) around stagnation with α-particle deposition turned off by the nonlocal model (solid lines) and the flux-limited SH model (dashed lines). The vertical dashed lines are on behalf of the moments of stagnation. (c) Distribution of the electron temperature T_e (red lines) and the mass density ρ (black lines) in the hot-spot and dense fuel shell at stagnation under the conditions of considering the nonlocal effects (solid) or not (dashed) and turning on the α-particle deposition (with stars) or not (without stars). (d) Evolution of the DT fusion power (black lines) by the nonlocal model (solid) and the flux-limited SH model (dashed), along with the final fusion yields (hollow triangles). The fusion power is defined as the energy released by DT fusion in unit time during the ignition stage.

adiabat of the fuel shell is still maintained at a high value due to the preheating, which is not conducive for the shell compression. Figure 3(b) plots the time evolution of the hot-spot pressure (brown lines) and the shell area density (green lines) around stagnation with the α-particle energy deposition turned off. We see clearly that the stagnation (corresponding the hot-spot pressure peak) is achieved much earlier from 19.92 to 19.7 ns and the coast time, which is defined as the time duration between the stagnation time and the laser shut-off time (18.2 ns), is reduced from 1.72 to 1.5 ns. Furthermore, the stagnation pressure is distinctly increased, as the brown lines show, by 18%, due to the contributions of more compressed and heated fuel and reduced coast time, which can help achieve the ignition threshold more easily [1]. However, the peak areal density ($\rho R_{\max}$) is essentially unchanged after considering the nonlocal effect, as the green lines show, which is the balanced result of more fuel compressed by the convergent shock and higher adiabat reducing the fuel compressibility.

Figure 3(c) shows the electron temperature T_e (red lines) and the mass density ρ (black lines) in the hot spot and dense fuel shell at stagnation. We see that a higher-temperature hot spot and a denser fuel shell are achieved owing to higher stagnation pressure and more compressed fuel, where the peak hot-spot temperature and the shell density both increase by about 10%. Moreover, Figure 3(d) presents that the fusion burning process becomes faster after considering the nonlocal effect, releasing 120 MJ (see the solid triangle symbol) of energy in a short fusion burn duration (with full width at half maximum 43 ps), while the simulation with the flux-limited SH model predicts a fusion yield of 115 MJ (see the dashed triangle symbol) with a fusion burn duration of 90 ps. It is worth noting that the reason that both cases achieve almost the same fusion yields is that in both cases the achieved peak areal densities of $\rho R_{\max} \sim 3.5$ g/cm^2 are similar, which determines the maximum burn-up fraction of the DT fuel [$\theta \approx 1/(1 + 7/\rho R_{\max})$] (in simulations it is about 26%, very close to the theoretical estimation of 33%). In short, although the final fusion yield for high-gain SAI design is almost unchanged, the coast time and the fusion burn duration are both reduced by the nonlocal effect, and the stagnation pressure is distinctly increased, potentially lowering the ignition threshold.

V. TIME-DELAY WINDOW AND INTENSITY RANGE FOR HIGH-GAIN SAI

Figure 4 shows the time-delay window between the igniter spike and the compression pulse and the intensity range of the igniter spike for achieving high-gain SAI, which determines the experimental feasibility and robustness of SAI. Figure 4(b) exhibits the quantitative fuel mass swept by the convergent shock after the collision for a series of laser pulse designs with different delay times partly shown in Fig. 4(a), with the 0.7-ns-dip setup defined as the zero point (corresponding to the simulation setup for which the maximum fusion yield is acquired). We see clearly that the shocked fuel mass (swept by the convergent shock after the collision) in simulations using the nonlocal model is obviously larger than that using the flux-limited SH model, which is the result of the shock collision occurring at a place farther away from the inner surface of the fuel shell as shown in Fig. 3(a). When the delay time is chosen as -0.3 ns, the collision almost occurs at the inner surface for the flux-limited SH model, while a relatively high fuel mass can be shocked and compressed for the nonlocal model, as shown in the inset. Therefore, a for short delay interval or a narrow dip, the nonlocal effect can effectively improve the burning performance by providing more fuel. Figure 4(c) depicts the corresponding yield curves as a function of the delay time: on the one hand, the maximum fusion yield is essentially unchanged as Fig. 3(d) indicates; on the other hand, the time-delay window for high-gain SAI ($G > 10$) is significantly broadened, from only 0.45 to 0.7 ns, which means that there is a wider range of delays between two pulses for which high gain is achieved. The broadened time window relaxes the difficulty of laser pulse shaping, within the capabilities of a no matter "full-quad" or "split-quad" scheme for the NIF [15].

Figure 4(d) shows the fusion yields as a function of the igniter spike intensity [the specific laser shapes are shown in the inset of Fig. 4(a)]: with the increase of the laser intensity, the fusion yields increase first and then decrease, presenting an intensity range for achieving high-gain SAI. The intensity range is significantly expanded to high-intensity for the nonlocal case, nearly 3 times wider than that by the flux-limited SH model, which suggests the intensity requirement for high-gain is significantly relaxed. In addition, the optimal

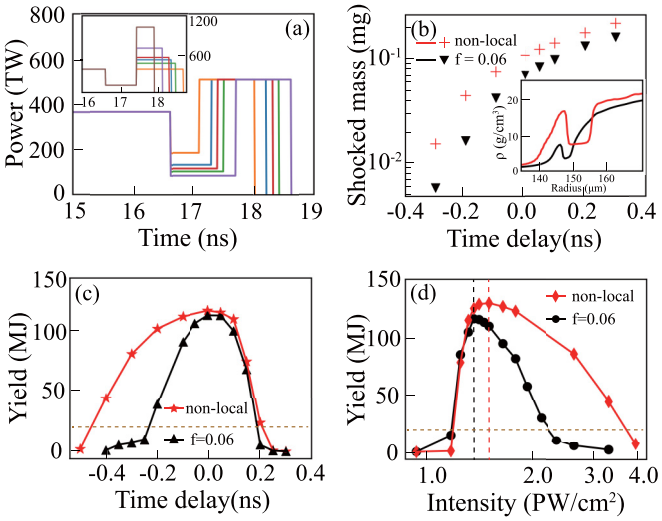

FIG. 4. Time-delay window between the igniter spike and the compression pulse and the intensity range of the igniter spike for achieving high-gain SAI after considering the nonlocal effects. (a) The laser pulse shapes with different time delays between the igniter spike and the compression pulse, with the total laser energy keeping 2.0 MJ and the igniter spike unchanged. The inset is the laser shapes with different intensities for the igniter spike. (b) The fuel mass shocked by the convergent shock after collision as a function of the time delay, in simulations using the nonlocal model (red cross) or flux-limited SH model (black inverted-triangle), with the 0.7-ns-dip setup defined as the 0-ns time delay. The inset presents the density profiles before shock collision in simulations with the time delay of −0.3 ns. (c) Thermonuclear energy yields as a function of the time delay in simulations using the nonlocal model (red line) or flux-limited SH model (black line), with the orange dashed line representing the fusion gain $G = 10$, above which we define as high gain. (d) Thermonuclear energy yield as a function of the intensity of the igniter laser, with the orange horizontal dashed line representing the fusion gain $G = 10$ (high gain) and vertical dashed lines on behalf of optimal laser intensities corresponding to maximum yields.

laser intensity is shifted up ∼12%, from 1.34×10^{15} to 1.5×10^{15} W/cm^2, which is reasonable because earlier shock rebound requires faster igniter shock to match and collide at proper positions. Note that for the igniter spikes with intensity $\leqslant 3.9 \times 10^{15}$ W/cm^2 in our SAI scheme, the negative impact of LPI is much weaker, compared to the conventional shock ignition scheme where the peak laser intensity $I \sim 10^{16}$ W/cm^2 is generally used. In our SAI cases, although LPI may slightly scatter the incident laser and slightly reduce the final fusion yield, its effect on the high-gain intensity range can be neglected (the high-gain intensity range is reduced by 7%; see details in the first section of the Supplemental Material [37]).

In addition, RTI is generally thought to significantly affect the implosion dynamics in direct-drive ICF. However, for SAI, due to its relatively low implosion velocity, the growth of RTI is greatly inhibited. Besides, the nonlocal thermal transport effects in SAI mainly modify the temperature of the fuel shell bulk and the place where shock collision occurs, which are basically unaffected by RTI. Therefore, including RTI will likely have little effect on the trends we have observed from adding nonlocal thermal transport (see details in the second section of the Supplemental Material [37]).

VI. CONCLUSION

In conclusion, we revisit the whole implosion and ignition dynamics of SAI by self-consistently including modeling of the nonlocal thermal transport effect into the radiation hydrodynamic simulations. We find that, due to the nonlocal effects, the implosion performance of SAI is improved and the laser shape requirement for high-gain fusion is reduced. On the one hand, the time-delay window between the igniter spike and the compression pulse for achieving high-gain fusion is much broadened from about 0.45 to 0.7 ns, easier to achieve in existing experimental devices such as NIF. On the other hand, both the coast time and the fusion burn duration are significantly reduced respectively from 1.72 ns down to 1.5 ns for the former and from 90 to 43 ps for the latter, with the stagnation pressure distinctly increased, potential to reach Lawson's criterion [1] more easily (lower ignition threshold). Therefore, after self-consistently modeling the nonlocal effects, SAI seems to be a more viable and promising scheme for future high-gain ICF.

ACKNOWLEDGMENTS

This work is supported by the National Key R&D Program of China, Grants No. 2022YFA1603200 and No. 2022YFA1603201; the National Natural Science Foundation of China, Grants No. 12135001, No. 11825502, and No. 11921006; and the Strategic Priority Research Program of CAS, Grant No. XDA25050900. B.Q. acknowledges support from the National Natural Science Funds for Distinguished Young Scholars, Grant No. 11825502. The simulations were carried out on the Tianhe-2 supercomputer at the National Supercomputer Center in Guangzhou.

[1] O. A. Hurricane, P. K. Patel, R. Betti, D. H. Froula, S. P. Regan, S. A. Slutz, M. R. Gomez, and M. A. Sweeney, Physics principles of inertial confinement fusion and U. S. program overview, Rev. Mod. Phys. **95**, 025005 (2023).

[2] J. Lindl, Development of the indirect-drive approach to inertial confinement fusion and the target physics basis for ignition and gain, Phys. Plasmas **2**, 3933 (1995).

[3] R. Betti and O. Hurricane, Inertial-confinement fusion with lasers, Nat. Phys. **12**, 435 (2016).

[4] J. Tollefson and E. Gibney, Nuclear-fusion lab achieves ignition: what does it mean? Nature (London) **612**, 597 (2022).

[5] H. Abu-Shawareb *et al.*, Lawson criterion for ignition exceeded in an inertial fusion experiment, Phys. Rev. Lett. **129**, 075001 (2022).

[6] A. Pak, L. Divol, D. T. Casey, S. F. Khan, A. L. Kritcher, J. E. Ralph, R. Tommasini, C. Trosseille, A. B. Zylstra, K. L. Baker, N. W. Birge, R. Bionta, B. Bachmann, E. L. Dewald,

T. Doeppner, M. S. Freeman, D. N. Fittinghoff, V. Geppert-Kleinrath, H. Geppert-Kleinrath, K. D. Hahn *et al.*, Dynamics and power balance of near unity target gain inertial confinement fusion implosions, Phys. Rev. Lett. **131**, 065101 (2023).

[7] R. S. Craxton, K. S. Anderson, T. R. Boehly *et al.*, Direct-drive inertial confinement fusion: A review, Phys. Plasmas **22**, 110501 (2015).

[8] J. Nuckolls, L. Wood, A. Thiessen *et al.*, Laser compression of matter to super-high densities: Thermonuclear (CTR) applications, Nature (London) **239**, 139 (1972).

[9] V. Gopalaswamy, R. Betti, J. P. Knauer *et al.*, Tripled yield in direct-drive laser fusion through statistical modelling, Nature (London) **565**, 581 (2019).

[10] D. Patel, J. P. Knauer, D. Cao, R. Betti, R. Nora, A. Shvydky, V. Gopalaswamy, A. Lees, S. Sampat, W. R. Donaldson, S. P. Regan, C. Stoeckl, C. J. Forrest, V. Y. Glebov, D. R. Harding, M. J. Bonino, R. T. Janezic, D. Wasilewski, C. Fella, C. Shuldberg *et al.*, Effects of laser bandwidth in direct-drive high-performance DT-layered implosions on the OMEGA laser, Phys. Rev. Lett. **131**, 105101 (2023).

[11] L. J. Perkins, R. Betti, K. N. LaFortune, and W. H. Williams, Shock ignition: A new approach to high gain inertial confinement fusion on the national ignition facility, Phys. Rev. Lett. **103**, 045004 (2009).

[12] R. Betti, C. D. Zhou, K. S. Anderson, J. L. Perkins, W. Theobald, and A. A. Solodov, Shock ignition of thermonuclear fuel with high areal density, Phys. Rev. Lett. **98**, 155001 (2007).

[13] X. Ribeyre, G Schurtz, M. Lafon *et al.*, Shock ignition: an alternative scheme for HiPER, Plasma Phys. Control. Fusion **51**, 015013 (2009).

[14] A. J. Schmitt, J. W. Bates, S. P. Obenschain *et al.*, Shock ignition target design for inertial fusion energy, Phys. Plasmas **17**, 042701 (2010).

[15] K. S. Anderson, R. Betti, P. W. McKenty *et al.*, A polar-drive shock-ignition design for the National Ignition Facility, Phys. Plasmas **20**, 056312 (2013).

[16] S. Atzeni, X. Ribeyre, G. Schurtz *et al.*, Shock ignition of thermonuclear fuel: principles and modelling, Nucl. Fusion **54**, 054008 (2014).

[17] D. Batani, S. Baton, A. Casner *et al.*, Physics issues for shock ignition, Nucl. Fusion **54**, 054009 (2014).

[18] D. Batani, L. Antonelli, F. Barbato *et al.*, Progress in understanding the role of hot electrons for the shock ignition approach to inertial confinement fusion, Nucl. Fusion **59**, 032012 (2019).

[19] V. T. Tikhonchuk, Physics of laser plasma interaction and particle transport in the context of inertial confinement fusion, Nucl. Fusion **59**, 032001 (2019).

[20] R. H. H. Scott, D. Barlow, W. Trickey, A. Ruocco, K. Glize, L. Antonelli, M. Khan, and N. C. Woolsey, Shock-augmented ignition approach to laser inertial fusion, Phys. Rev. Lett. **129**, 195001 (2022).

[21] S. X. Hu, L. Ceurvorst, J. L. Peebles, A. Mao, P. Li, Y. Lu, A. Shvydky, V. N. Goncharov, R. Epstein, K. A. Nichols, R. M. N. Goshadze, M. Ghosh, J. Hinz, V. V. Karasiev, S. Zhang, N. R. Shaffer, D. I. Mihaylov, J. Cappelletti, D. R. Harding, C. K. Li *et al.*, Laser-direct-drive fusion target design with a high-Z gradient-density pusher shell, Phys. Rev. E **108**, 035209 (2023).

[22] D. T. Michel, A. K. Davis, V. N. Goncharov, T. C. Sangster, S. X. Hu, I. V. Igumenshchev, D. D. Meyerhofer, W. Seka, and D. H. Froula, Measurements of the conduction-zone length and mass ablation rate in cryogenic direct-drive implosions on OMEGA, Phys. Rev. Lett. **114**, 155002 (2015).

[23] O. V. Gotchev, V. N. Goncharov, J. P. Knauer, T. R. Boehly, T. J. B. Collins, R. Epstein, P. A. Jaanimagi, and D. D. Meyerhofer, Test of thermal transport models through dynamic overpressure stabilization of ablation-front perturbation growth in laser-driven CH foils, Phys. Rev. Lett. **96**, 115005 (2006).

[24] S. P. Regan, R. Epstein, V. N. Goncharov *et al.*, Laser absorption, mass ablation rate, and shock heating in direct-drive inertial confinement fusion, Phys. Plasmas **14**, 056305 (2007).

[25] Z. H. Chen, X. H. Yang, G. B. Zhang *et al.*, Effect of non-local transport of hot electrons on the laser target ablation, Phys. Plasmas **30**, 062710 (2023).

[26] G. P. Schurtz, Ph. D. Nicolaï and M. Busquet, A nonlocal electron conduction model for multidimensional radiation hydrodynamics codes, Phys. Plasmas **7**, 4238 (2000).

[27] M. Sherlock, J. P. Brodrick, C. P. Ridgers *et al.*, A comparison of non-local electron transport models for laser-plasmas relevant to inertial confinement fusion, Phys. Plasmas **24**, 082706 (2017).

[28] A. R. Bell and M. Tzoufras, Electron transport and shock ignition, Plasma Phys. Control. Fusion **53**, 045010 (2011).

[29] A. Marocchino, S. Atzeni and A. Schiavi, Effects of non-local electron transport in one-dimensional and two-dimensional simulations of shock-ignited inertial confinement fusion targets, Phys. Plasmas **21**, 012701 (2014).

[30] A. Sunahara, J.A. Delettrez, C. Stoeckl, R.W. Short, and S. Skupsky, Time-dependent electron thermal flux inhibition in direct-drive laser implosions, Phys. Rev. Lett. **91**, 095003 (2003).

[31] S. X. Hu, V. A. Smalyuk, V. N. Goncharov, S. Skupsky, T. C. Sangster, D. D. Meyerhofer, and D. Shvarts, Validation of thermal-transport modeling with direct-drive, planar-foil acceleration experiments on OMEGA, Phys. Rev. Lett. **101**, 055002 (2008).

[32] K. Falk, M. Holec, C. J. Fontes, C. L. Fryer, C. W. Greeff, H. M. Johns, D. S. Montgomery, D. W. Schmidt, and M. Smid, Measurement of preheat due to nonlocal electron transport in warm dense matte, Phys. Rev. Lett. **120**, 025002 (2018).

[33] J. P. Brodrick, R. J. Kingham, M. M. Marinak *et al.*, Testing nonlocal models of electron thermal conduction for magnetic and inertial confinement fusion applications, Phys. Plasmas **24**, 092309 (2017).

[34] B. Fryxell, K. Olson, P. Ricker *et al.*, FLASH: An adaptive mesh hydrodynamics code for modeling astrophsical thermalnuclear flashes, Astrophys. J. Suppl. Ser. **131**, 273 (2000).

[35] Jr. L. Spitzer and R. Härm, Transport phenomena in a completely ionized gas, Phys. Rev. **89**, 977 (1953).

[36] R. C. Malone, R. L. McCrory, and R. L. Morse, Indications of strongly flux-limited electron thermal conduction in laser-target experiments, Phys. Rev. Lett. **34**, 721 (1975).

[37] See Supplemental Material at http://link.aps.org/supplemental/10.1103/PhysRevResearch.6.013332 for specific evaluations of the negative impacts of Laser-plasma instabilities (LPI) and Rayleigh-Taylor instability (RTI) on the physical results and trends we have observed from adding nonlocal thermal transport in the Shock-Augmented Ignition (SAI) scheme.